INTERFACE

rsif.royalsocietypublishing.org

Research

Cite this article: Ramesh K, Melzner F, Griffith AW, Gobler CJ, Rouger C, Tasdemir D, Nehrke G. 2018 *In vivo* characterization of bivalve larval shells: a confocal Raman microscopy study. *J. R. Soc. Interface* **15**: 20170723.
http://dx.doi.org/10.1098/rsif.2017.0723

Received: 3 October 2017
Accepted: 16 March 2018

Subject Category:
Life Sciences–Earth Science interface

Subject Areas:
biochemistry, biomaterials

Keywords:
aragonite, larval shell, mussel

Author for correspondence:
Kirti Ramesh
e-mail: kramesh@geomar.de

Electronic supplementary material is available online at https://dx.doi.org/10.6084/m9.figshare.c.4040681.

THE ROYAL SOCIETY PUBLISHING

In vivo characterization of bivalve larval shells: a confocal Raman microscopy study

Kirti Ramesh[1], Frank Melzner[1], Andrew W. Griffith[2], Christopher J. Gobler[2], Caroline Rouger[1], Deniz Tasdemir[1] and Gernot Nehrke[3]

[1]Marine Ecology, GEOMAR Helmholtz Centre for Ocean Research Kiel, Germany
[2]School of Marine and Atmospheric Sciences, Stony Brook University, Stony Brook, NY, USA
[3]Alfred Wegener Institute for Polar and Marine Research, Am Handelshafen 12, Bremerhaven, Germany

KR, 0000-0001-7889-6722; CJG, 0000-0002-7576-8079

In vivo confocal Raman microscopy (CRM), polarized light microscopy and Fourier transform infrared spectroscopy (FTIR) were used to determine if a significant amount of amorphous calcium carbonate (ACC) exists within larval shells of Baltic mytilid mussels (*Mytilus edulis*-like) and whether the amount of ACC varies during larval development. No evidence for ACC was found from the onset of shell deposition at 21 h post-fertilization (hpf) until 48 hpf. Larval *Mytilus* shells were crystalline from 21 hpf onwards and exhibited CRM and FTIR peaks characteristic of aragonite. Prior to shell deposition at 21 hpf, no evidence for carbonates was observed through *in vivo* CRM. We further analysed the composition of larval shells in three other bivalve species, *Mercenaria mercenaria*, *Crassostrea gigas* and *Crassostrea virginica* and observed no evidence for ACC, which is in contrast to previous work on the same species. Our findings indicate that larval bivalve shells are composed of crystalline aragonite and we demonstrate that conflicting results are related to sub-optimal measurements and mis-interpretation of CRM spectra. Our results demonstrate that the common perception that ACC generally occurs as a stable and abundant precursor during larval bivalve calcification needs to be critically reviewed.

1. Introduction

Molluscan larvae, whose calcium carbonate shells provide structural support and protection, exhibit much higher relative calcification rates than adult forms [1]. High energetic costs of larval bivalve calcification likely arise from the transport and accumulation of calcification substrates (calcium and bicarbonate), the excretion of protons, which are generated during shell formation, as well as shell organic matrix synthesis [2,3]. This high energetic investment renders them vulnerable to environmental disturbances such as ocean acidification [2,4,5]. The biological control and structural diversity of shell formation in molluscs has received much attention because a better understanding of biomineralization processes is crucial to understand vulnerability to abiotic stressors [1,6–9]. Despite the high diversity in shell structure and polymorph composition found in adult bivalve shells, calcification during larval development is morphologically similar between species. Cell lineages involved in shell formation are homologous and exhibit a similar enzymatic histochemistry [10]. Furthermore, preceding shell formation, the cellular differentiation processes of shell-forming cells are conserved in bivalve species [11,12]. In bivalves, ectodermal cells in the dorsal region thicken and invaginate to form the shell gland [10]. A subsequent evagination of the shell gland and flattening of ectodermal cells gives rise to the so-called shell field [10]. Initial shell mineralization in bivalve molluscan larvae takes place during the trochophore larval stage, within the shell field region [13]. The shell field evaginates during the trochophore stage and the surrounding epithelia secrete an early organic layer which is assumed to protect the first shell structures from dissolution during adverse environmental conditions such as lowered saturation state for aragonite

[2,13]. This early organic layer is continually mineralized as it spans over the surface of the larval body, with a small fraction that remains unmineralized at the growing edge of the shell [14]. Shell calcification laterally compresses the larva and the epithelial cells within the shell field are presumably responsible for the secretion of the first larval shell, prodissoconch I (PD I, D-veliger stage) [15]. At this early stage, the shell is composed solely of aragonite [16–19]. The formation of PD I is followed by the secretion of prodissoconch II (PD II, veliger stage), which is characterized by the presence of growth lines. The shell-forming epithelial cells within the shell field ultimately differentiate into the shell-forming organ in juveniles and adults, the mantle. Following metamorphosis from the (pedi)veliger stage to juveniles, the mantle secretes new shell layers (dissoconch) at the edge of prodissoconch II that formed previously [11,20].

Adult and juvenile mytilid shells consist of two distinct layers that are composed of different calcium carbonate polymorphs: aragonitic tablets (inner nacreous layer) and calcitic prisms (outer layer) [21]. However, within the first 2 days of development, larval bivalves rapidly secrete aragonitic shells, the mass of which corresponds to approximately 90% of their somatic body mass [2]. This shell deposition process must involve a rapid accumulation and transport of calcium and carbonate ions to the shell field region. Organisms may use transepithelial transport (cellular and paracellular pathways) to enable accumulation of calcium and carbonate ions directly at the site of calcification. Alternatively, amorphous calcium carbonate (ACC) precursor phases could be accumulated intracellularly to be exocytosed onto the growing shell [22]. Such a mechanism has been demonstrated in larval echinoderms, where intracellular vesicles containing calcium carbonate are widely distributed across the larva and are subsequently deposited onto the larval spicules [23]. Such detailed understanding is lacking in mollusc larval stages. Analysis of larval bivalve shells (*Mercenaria mercenaria*, *Crassostrea gigas*) using Raman and infrared spectroscopy has also suggested the presence of an ACC precursor phase [24]. However, more recently, lack of evidence of ACC in the larval shells of oysters based on focused ion beam transmission electron microscopy (FIB-TEM) techniques [25,26] has necessitated a review of occurrence of ACC in larval shell carbonates molluscs. Recent studies have exclusively observed the presence of crystalline aragonite in the veliger larvae of the oysters *Crassostrea nippona* and *Pinctada fucata*, with no evidence for the intermittent presence of an ACC phase [25,26]. The advantage of using amorphous precursors such as ACC during calcification is that they may be moulded into intricate structures and their isotropic nature allows for mechanical strain in all directions [27]. ACC is a highly unstable polymorph of calcium carbonate and its solubility is almost 30 times higher than that of aragonite [4,28]. Therefore, an understanding of its role in biomineralization is crucial for predicting the vulnerability of early calcification processes to environmental disturbances, in particular of the oceanic carbonate system [1,2].

The conflicting results mentioned above illustrate the need for studying more molluscan species using a variety of methodological approaches. Here, we address the question whether ACC is a precursor phase involved in mytilid mussel shell formation using *in vivo* confocal Raman microscopy (CRM) for the first time. CRM offers a high-spatial resolution (sub-micron) to follow the initial appearance of crystalline structures and to determine their phase composition from the earliest calcifying stages (trochophore stages) to D-veligers and freshly settled juveniles. In addition, we present results from Fourier transform infrared (FTIR) spectroscopy on *Mytilus* D-veliger shells and CRM analyses on larval shells from three additional bivalve species, *M. mercenaria*, *C. gigas* and *Crassostrea virginica* to investigate the role of ACC in bivalve larval shell formation. Finally, we follow the deposition of polyenes (pigments) within the shell during initial calcification in trochophore larvae, using CRM.

2. Material and methods

2.1. Animal collection and larval culture

Adult and juvenile mussels *Mytilus* were collected in Kiel Fjord (54°19.8′ N; 10°9.0′ E) in June 2015 and 2016. Kiel mytilids are *Mytilus edulis* × *trossulus* hybrids similar to *M. edulis*. We will refer to them as Baltic *M. edulis*-like according to Stuckas *et al.* [29]. Adult animals were spawned as described previously, at pH_{NBS} 8.1 and a salinity of 16 psu [14]. Larvae were maintained at GEOMAR at 17°C until 48 h post-fertilization (hpf). Larvae from five separate fertilizations were analysed for the presence of ACC, aragonite and calcite. Adult Pacific oysters, *C. gigas* were collected from Sylt, Germany and spawned as described previously [30] at pH_{NBS} 8.20 and a salinity of 34 psu. Larval cultures were maintained at GEOMAR at 22°C until 24 hpf, when D-veliger stages were reached. Adult hard clams, *M. mercenaria* were obtained from Ocean Rich distributors (Brookhaven, NY, USA) and adult Eastern oysters, *C. virginica* were obtained from the Shinnecock Bay Restoration Program (NY, USA; 40°51′50.4″ N; 72°29′27.6″ W). Adult *M. mercenaria* and *C. virginica* were spawned as described previously at pH_{NBS} 8.12 and a salinity of 30 psu [31]. Larval cultures were maintained at 24°C until 12 days post-fertilization (dpf, *M. mercenaria*) and 10 dpf (*C. virginica*) at Stony Brook University's Southampton Marine Sciences Center (Southampton, NY, USA). Baltic *M. edulis*-like larvae were analysed alive and frozen, whereas larvae of *M. mercenaria*, *C. gigas* and *C. virginica* were analysed frozen. Frozen larval samples were brought to room temperature and Raman spectra were collected on samples within 30 min. CRM analyses were performed on samples within three months of sample collection. Samples of *M. mercenaria* and *C. virginica* were transferred to GEOMAR, Kiel from the USA on dry ice. Specimens of Baltic *M. edulis*-like juveniles were collected in Kiel Fjord (54°19.8′ N; 10°9.0′ E) in August 2015. Samples were flash frozen in liquid nitrogen and stored at −20°C until further use.

2.2. Confocal Raman microscopy

To investigate the calcium carbonate polymorphs present during shell formation of Baltic *M. edulis*-like, we used a WITec alpha 300R (WITec GmbH, Germany) confocal Raman microscope (CRM) equipped with a 488 nm laser diode housed at the Alfred Wegener Institute in Bremerhaven. An ACC standard was prepared at 1°C according to the method described in Rodriguez-Blanco *et al.* [32]. Briefly, equal volumes of cooled (1°C) 10 mM $CaCl_2$ and Na_2CO_3 solutions were combined and the resulting suspension was vacuum filtered (0.2 µm). Stable ACC as described in [32] was recovered by washing the filtered solids with isopropanol and drying them in air. Reference spectra of calcite (Iceland spar) and aragonite (single crystal, Spain) were obtained using in-house standards also reported in a previous publication [33]. An ACC–aragonite mixture was prepared by mixing equal masses of powdered ACC and aragonite standards using a pestle and mortar. The resulting mixture was placed between a glass slide and coverslip and mapped using CRM to demonstrate the ability of the technique to discriminate between

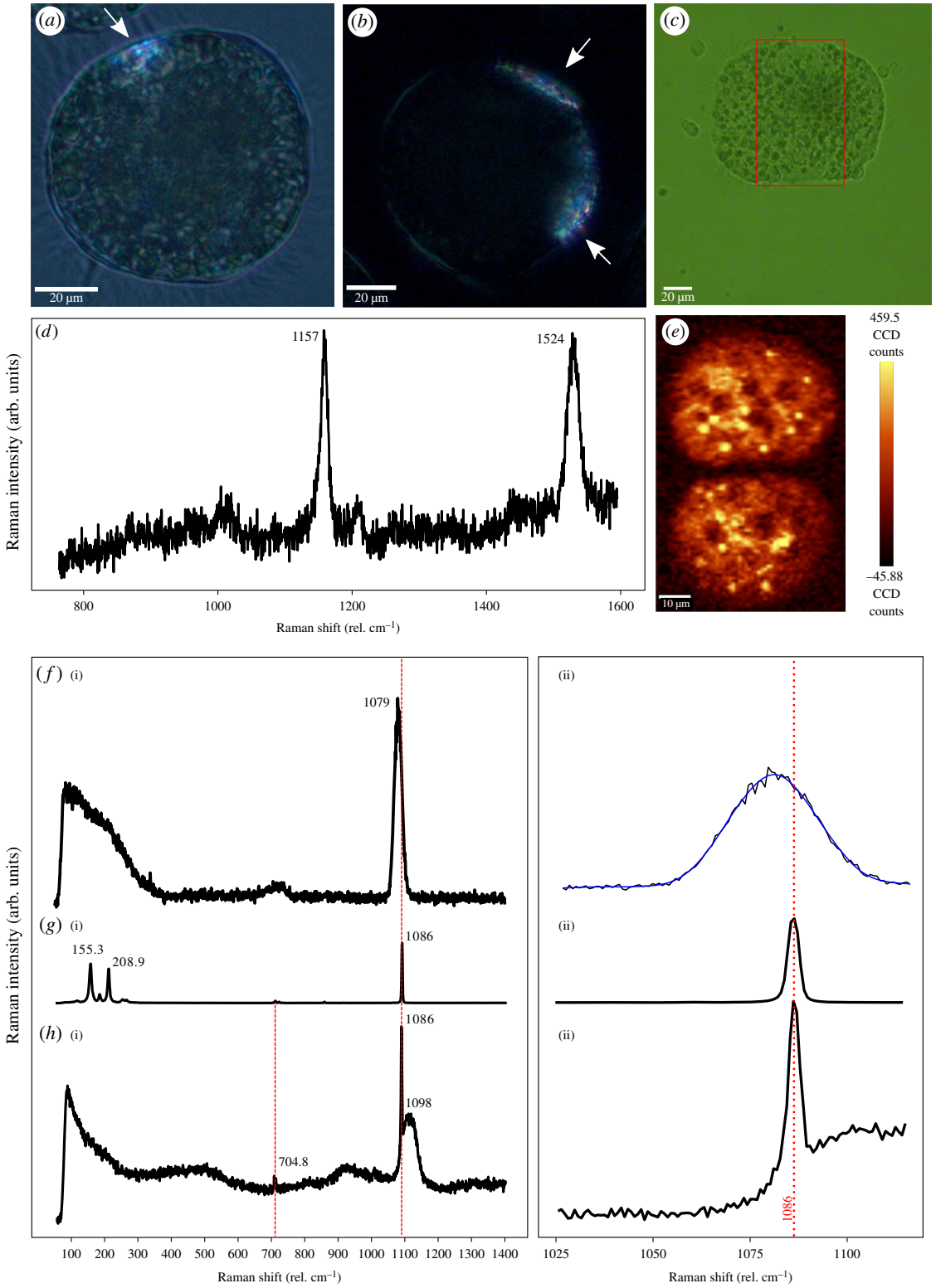

Figure 1. Trochophore shell deposition in Baltic *Mytilus edulis*-like using polarized light and CRM. (*a*,*b*) Birefringent shells are denoted by arrows in trochophore larvae (21 hpf). (*c*) Transmission image of a calcifying trochophore larva at 21 hpf in dorsal view. The boxed region was subjected to a Raman scan. (*d*) Raman spectra of the organic shell cover in focal plane, prior to shell deposition at 20 hpf. (*e*) Raman scan for the boxed region in (*c*) was integrated for CO_3^{2-} -stretching (1082.5–1087.5 rel. cm^{-1}). (*f*(i)) Raman spectrum of an ACC standard. (*g*(i)) Raman spectrum of an aragonite standard. (*h*(i)) Raman spectrum of an *in vivo* trochophore larval shell. (*f*(ii)) The CO_3^{2-}-stretching mode of ACC in (*f*(i)). (*g*(ii)) The CO_3^{2-}-stretching mode of aragonite in (*g*(i)). (*h*(ii)) The CO_3^{2-}-stretching mode of an *in vivo* trochophore shell in (*h*(i)) to illustrate the presence of aragonite-specific CO_3^{2-}-stretching in the shell.

multiple calcium carbonate polymorphs in a sample. Initial analyses were performed on previously frozen, 48 hpf D-veliger Baltic *M. edulis*-like larvae that were stored and prepared as described by Weiss *et al*. [24]. In brief, 48 hpf larvae were shock-frozen in liquid nitrogen and stored at −20°C until further use. Samples were thawed at room temperature and analysed wet on calcium fluoride discs (Korth Kristalle GmbH, Germany).

In vivo Raman measurements were performed on Baltic *M. edulis*-like larvae between 20 and 48 hpf. The same samples investigated by means of CRM *in vivo* measurements were characterized using a Zeiss Axio Scope.A1 polarized light microscope, located beside the CRM instrument. *In vivo* measurements on individual larvae at the CRM were performed for up to 1 h and the vitality of larvae was ensured by visual observation of

Table 1. Characteristic Raman shifts of calcium carbonate polymorphs and polyene pigments.

sample	characteristic wavenumber (cm^{-1})	references
ACC CO_3 stretching	1079	Raz *et al*. [28]
aragonite CO_3 stretching	1085–1087	Urmos *et al*. [39]
calcite CO_3 stretching	1086–1087	Urmos *et al*. [39]
ACC lattice vibrations	150–250	Raz *et al*. [28]
aragonite lattice vibrations	155, 206 and double peaks at 704	Nehrke *et al*. [36]
calcite lattice vibrations	156, 282 and 711	Nehrke *et al*. [36]
Mytilus edulis polyenes	1098 and 1484	Hedegaard *et al*. [34]

ciliary movement. Larvae were concentrated in filtered seawater (0.2 µm) using a 20 µm sieve. The drop containing the larvae (approx. 30 µl) was sandwiched between a glass slide and a glass coverslip, using cotton fibres as a spacer to prevent damage and confine the larvae in a hydrated environment. CRM measurements on Baltic *M. edulis*-like shells exhibited the presence of the typical Raman peaks associated with polyenes [24]. The polyene-related Raman peak in Baltic *M. edulis*-like (at 1098 rel. cm^{-1}) occurs very close to the position of the strongest carbonate peak for calcite and aragonite (1086 rel. cm^{-1}) (e.g. [34,35]). High spectral resolution grids (grating with 1800 and 2400 g mm^{-1}, BLZ 500 nm) were used to resolve these peaks. Resin-embedded (Araldite 2020, Huntsman International LLC, USA), polished cross-sections of freshly settled juveniles from Kiel Fjord were used to study the transition zone of the larval shell to the dissonconch. Prior to embedding, juvenile *M. edulis*-like samples were brought to room temperature. Individual juvenile *M. edulis*-like samples were positioned in Araldite 2020 resin for embedding. Cross-sections of juvenile Baltic *M. edulis*-like resin-embedded shells were ground on a LOGITECH PM2A Precision Lapping/Polishing Machine using waterproof silicon carbide paper in the qualities of P1200, P2400, P4000 (Struers, Denmark). This grinding step was followed by a polishing step using a Struers diamond suspension of 3 µm and subsequent rinsing of the sample using de-ionized water. A detailed description of the method used to map and identify the calcium carbonate polymorph distribution by CRM was described elsewhere [36,37]. Briefly, Raman scans were performed using a motorized scan table and spectra were acquired with an integration time of between 0.5–1 s. Identification of calcium carbonate polymorphs was based on the characteristic peak positions of lattice vibrational modes and CO_3^{2-} symmetric stretch. Raman spectra for frozen D-veliger larvae of the three additional species were collected on wet samples using a water immersion objective (Nikon, NIR APO 60×, WI NA 1.0). The theoretical lateral and axial resolutions for this objective are 250 and 430 nm, respectively. The *in vivo* CRM measurements (larval samples) were performed using a 20× objective (Zeiss, LD Plan NeoFluar NA 0.4). Juveniles were measured using the 20× objective having a numerical aperture of 0.4. For each sample, 5–10 spectra were acquired along a transect across the longitudinal section of the shell. Spectral analysis and image processing were performed using WITec Project software v. 2.04 (WITec GmbH, Germany). Spectra collected from single pixel positions were plotted using R (v. 3.3.2, R Development Core Team, R: http://www.R-project.org/.2011) and packages ggpmisc, ggplot2 and ggspectra.

2.3. Replication

In vivo CRM spectra were collected from $N = 16$ Baltic *M. edulis*-like larvae: four larvae at both 20 and 21 hpf, three at 25 hpf and five at 28 hpf. At least three positions on the shell of each larva were analysed. For analyses on frozen D-veligers, spectra were collected from 15, five, four and five larvae of Baltic *M. edulis*-like, *M. mercenaria*, *C. virginica* and *C. gigas*, respectively, with spectra taken from four to eight positions of the shell, per larva. CRM spectra were collected from three juvenile animals at five to 10 positions along the shell.

2.4. Fourier transform infrared spectroscopy

Reference spectra were measured for powdered aragonite and ACC standards that were prepared or acquired as described above. Infrared absorption spectra for larval shells were obtained according to Weiss *et al*. [24]. Briefly, ca. 100 000 Baltic *M. edulis*-like larvae were harvested at 48 hpf and shock-frozen in liquid nitrogen. Samples were stored at −20°C for subsequent analyses and thawed at room temperature prior to use. Whole larvae were treated with 2.5% sodium hypochlorite for 7 min followed by three rinses in de-ionized water to remove organic tissue [38]. The tissue-free larval shells were subsequently air-dried and ground to a fine powder using a plastic pestle suitable for Eppendorf tubes. FTIR spectra were collected using a Spectrum Two FT-IR spectrometer (Perkin Elmer), equipped with a UATR (single reflection diamond) on dried larval shell powder. Spectra were obtained in the range of 450–4000 cm^{-1} and Spectrum 10 software was used to perform background subtractions.

3. Results

3.1. *In vivo* confocal Raman microscopy analyses of larval shell composition

The initial larval shell formation was detected at 21 hpf by using the birefringence of aragonite observed between crossed polarizers (figure 1*a*, [13]). The birefringence increased gradually and was observed for both shell valves (arrows in figure 1*b*). The mineralized shell entirely covered the embryo surface after 48 hpf. No birefringence was observed before 21 hpf, indicating the absence of a shell. However, larvae exhibited an evagination of the shell field, which has been previously been determined to be related to the presence of an early organic layer between 18 and 20 hpf [14]. Raman spectral analysis of the region of the shell field prior to calcification at 18 hpf, using multiple point measurements, revealed characteristic spectra for organic pigments at 1157 and 1524 rel. cm^{-1} (figure 1*d*). Spectra of organic shell polyenes following calcification in Baltic *M. edulis*-like larval shells showed peaks at 1098 and 1479 rel. cm^{-1} (electronic supplementary material, figure S1).

We next analysed the larval shells at their earliest presence and followed their growth. In order to identify the

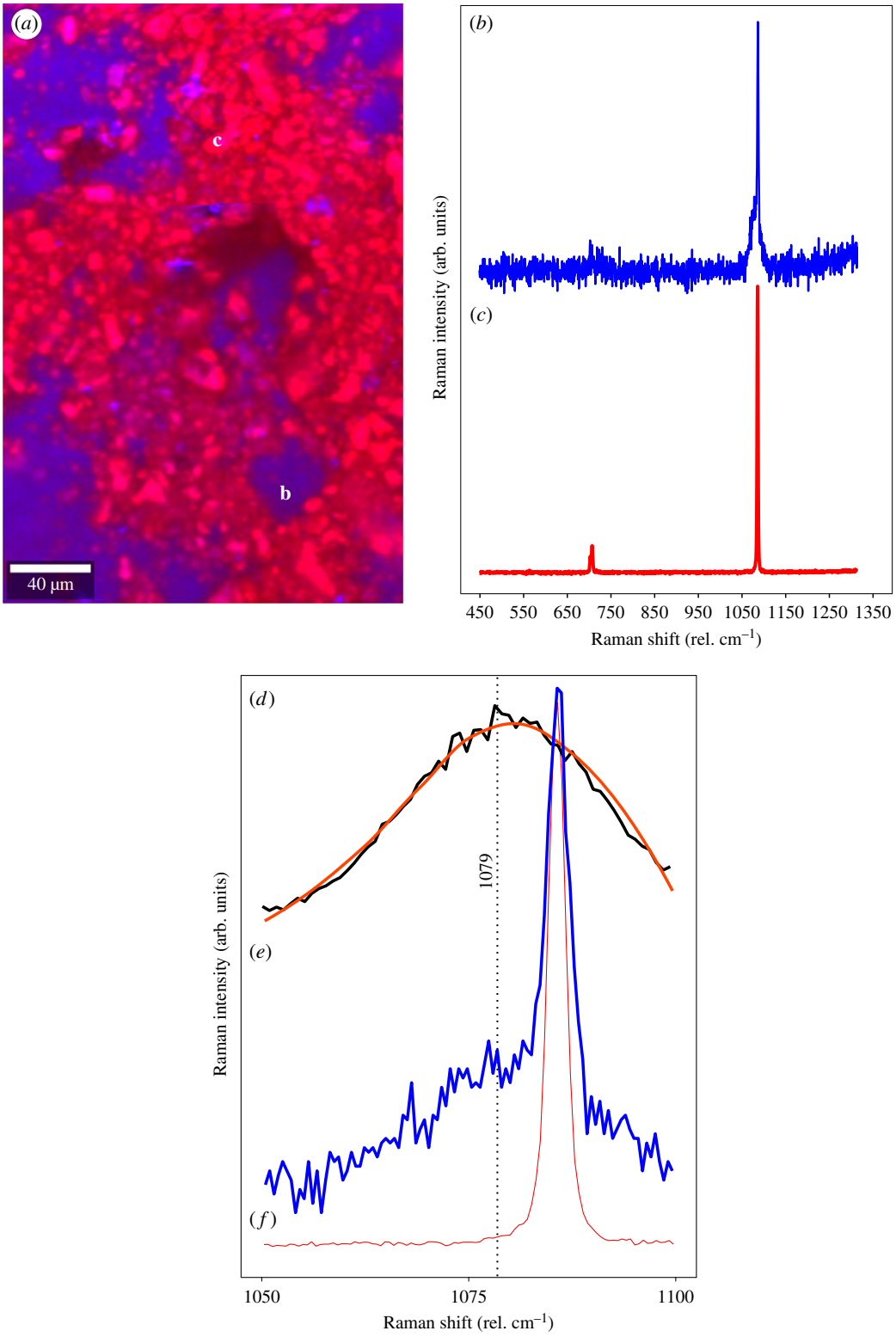

Figure 2. Confocal Raman microscopy analyses of an ACC–aragonite mixture. (*a*) Raman scan of ACC–aragonite mixture that was integrated for CO_3^{2-}-stretching mode of both polymorphs (red, aragonite, 1080.4–1090.4 rel. cm^{-1}) (blue, ACC, 1070.6-1075.6 cm^{-1}). (*b*,*c*) Raman spectra of ACC and aragonite in the mixture at positions 'b' and 'c' in (*a*), respectively, to illustrate the sensitivity of CRM techniques to detect the presence of multiple polymorphs on a sub-micron scale. (*d*) The CO_3^{2-}-stretching mode of the ACC standard. (*e*,*f*) Raman spectra of the CO_3^{2-}-stretching mode presented in (*b*) and (*c*), respectively.

occurrence of ACC, we measured an ACC standard (showing a characteristic Raman peak at 1079 rel. cm^{-1}, figure 1F1, 1F2, table 1) and aragonite and calcite standards showing characteristic peaks for aragonite at 155.3, 208.9 rel. cm^{-1} and 1086 rel. cm^{-1} with double peaks at 702.6 and 704.8 rel. cm^{-1} (figure 1G1, 1G2, table 1) and characteristic peaks for calcite at 156, 283.1 and 1087 rel. cm^{-1} (table 1). The standards were measured under the same conditions (laser intensity, pinhole) as the samples to guarantee comparability. Note the difference of seven to eight wavenumbers between the spectra of ACC and crystalline phases for the carbonate stretching mode (1079 (ACC) versus 1086 (aragonite), figure 1F2, 1G2). This difference in stretching mode is due to the fact that each calcium carbonate polymorph has a unique set of Raman bands, related to their unique structure. The bond length, bond strength and thus the

structural neighbourhood around the CO_3^{2-} groups differ, resulting in different positions of the Raman peaks [36,39]. A Raman spectrum obtained from a sample in which two phases are present will result in a spectrum that exhibits the peaks of both phases, but peaks will not merge into one peak with an intermediate peak position. We prepared and mapped an ACC–aragonite mixture to highlight the suitability of the CRM techniques to detect multiple phases present in a sample, on a sub-micron scale using appropriate grids (2400 g mm^{-1}, BLZ 500 nm). Figure 2 demonstrates the suitability of CRM techniques to accurately distinguish peak positions of the v_1 carbonate stretching mode in the ACC–aragonite mixture mapped, where the presence of ACC can be inferred from the asymmetric shape of the v_1 peak due to the addition of the characteristic v_1 band of ACC at 1079 rel. cm^{-1} (figure 2*b–f*). Similar asymmetric v_1 peaks were found by Jacob *et al.* [40] when studying ACC–crystalline carbonate mixtures present in the sternum of the isopod, *Porcellio scaber*.

In vivo CRM spectral analyses of Baltic *M. edulis*-like trochophore larval shells at 21 hpf reveal peaks at 703.1–703.8 and 1086 rel. cm^{-1}, indicating the presence of only aragonite in shell carbonates at the onset of shell formation (electronic supplementary material, figure S2). The larval shell at the PD I stage (48 hpf, 106 ± 2.3 µm length, figure 3*a*) shows characteristic aragonite peaks at 155, 207, 704 and 1087 rel. cm^{-1} (figure 3*d*). Figure 1*e* shows the Raman spectral map for the carbonate stretching mode (1082.5–1087.5 rel. cm^{-1}) for the boxed region of a trochophore larva at 21 hpf in figure 1*c*. In addition, CRM spectra revealed strong peaks at 1098 rel. cm^{-1} which is a reported polyene pigment peak specific to *M. edulis* shells [34,35]. All specimens examined exclusively contained aragonite in their larval shell. There was no evidence for the presence of ACC in the spectral analyses of Baltic *M. edulis*-like larval shells from the onset of calcification at 21–48 hpf.

3.2. Confocal Raman microscopy analyses on previously frozen larval shells

In order to test whether ACC precursors form the bulk of PD I larval shell carbonates in other bivalve species, we investigated Raman spectra of three additional larval bivalve species, *M. mercenaria*, *C. gigas* and *C. virginica*. The spectra from all three species exclusively revealed peaks at 155, 208, 703 and 1086 rel. cm^{-1} indicative of crystalline aragonite in the PD I shell (figure 4*a–g*).

3.3. Confocal Raman microscopy analyses on resin-embedded juveniles

A two-dimensional Raman map was obtained for the cross-section of the juvenile Baltic *M. edulis*-like shell to map the distribution of calcium carbonate polymorphs (figure 5*a*). The larval prodissoconchs clearly show the characteristic Raman peaks of aragonite at 155, 207 and 1087 rel. cm^{-1} (figure 5*e*, red). For the transition from aragonite to calcite, we recorded peaks specific to aragonite and calcite, indicating that the two polymorphs exist as distinct phases in the shell with no signs for ACC phases at the layer boundaries (figure 5). The transformation to a calcitic shell marks the start of the dissoconch with characteristics calcitic peaks at 156, 282 and 1087 rel. cm^{-1} (figure 5*f*, blue).

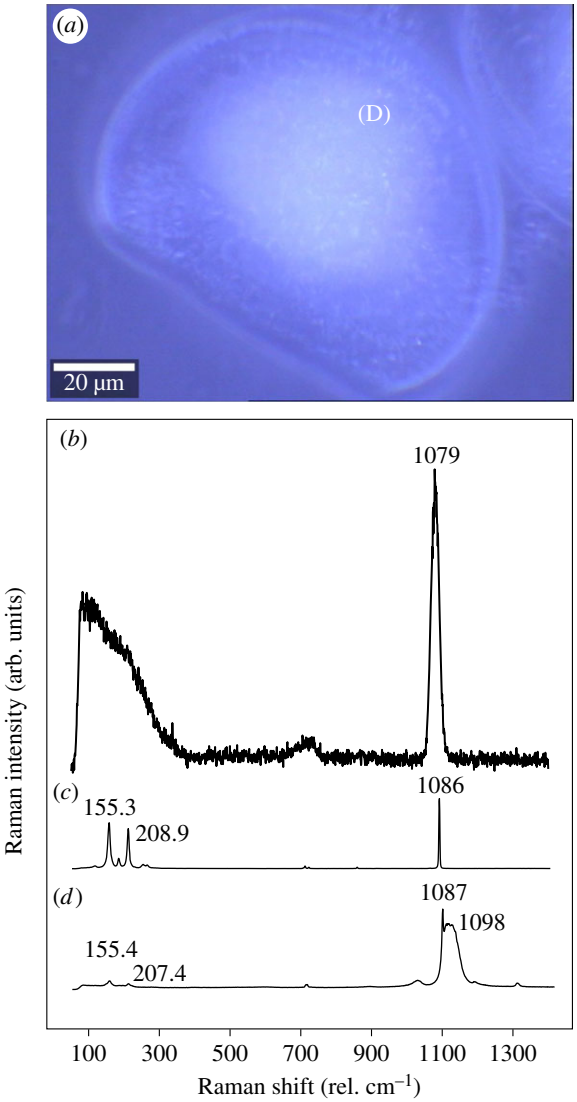

Figure 3. Prodissoconch I shell deposition in Baltic *Mytilus edulis*-like using CRM. (*a*) Transmission image of a D-veliger larva at 48 hpf in lateral view, for which multiple point Raman spectra were acquired. (*b*) Raman spectrum of an ACC standard. (*c*) Raman spectrum of an aragonite standard. (*d*) Raman spectrum collected at a single point on the D-veliger larval shell in (*a*) at point 'D'.

3.4. Additional measurements using Fourier transform infrared spectroscopy

The aragonite standard exhibited characteristic peaks of crystalline calcium carbonate polymorphs with distinct bands at 713 cm^{-1} (v_4), 860 cm^{-1} (v_2), a small band at 1086 cm^{-1} (v_1) and a large vibration between 1440 and 1500 cm^{-1} (v_3) (figure 6). FTIR spectra of the ACC standard are characterized by the lack of the vibration at v_4 region (713 cm^{-1}, figure 6) which is attributed to the OCO bending [41], consistent with previous research [42,43]. Bulk measurements of Baltic *M. edulis*-like larval shell samples revealed peaks at 713 and 860 cm^{-1} indicative of crystalline aragonite (figure 6).

4. Discussion

4.1. Polymorph composition of the shell

In this study, we aimed to clarify whether ACC plays a major role in larval shell formation in Baltic blue mussels

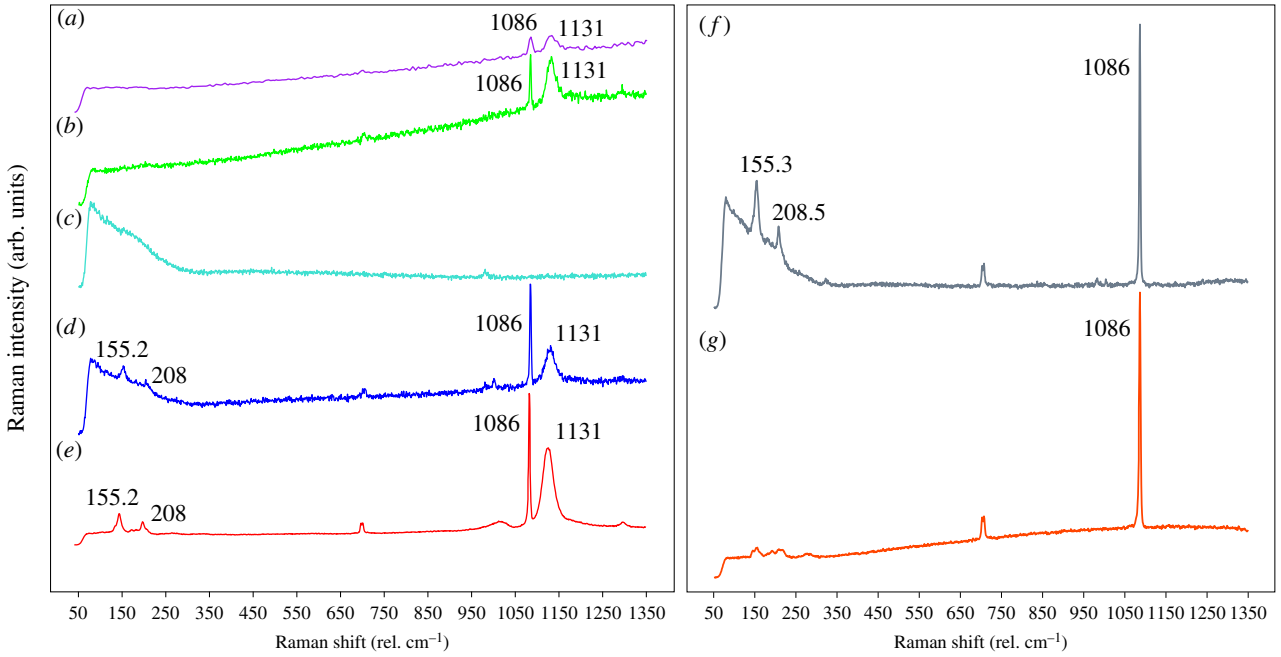

Figure 4. Raman spectra acquired from the veliger larval shells of three different larval species. (*a*) Raman spectrum of a *M. mercenaria* larval shell acquired using a 20× objective and a grid 600 g mm^{-1}, BLZ 500 nm. (*b*) Raman spectrum of a *M. mercenaria* larval shell acquired using a 20× objective and a grid 1800 g mm^{-1}, BLZ 500 nm. (*c*) Raman spectra of seawater acquired using the 60× water immersion objective to illustrate the similarity of peak positions of water and ACC peaks between 75 and 225 rel. cm^{-1}. (*d*) Raman spectra at the outer surface of a *M. mercenaria* larval shell acquired using the 60× water immersion objective. (*e*) Raman spectra at the focal plane of the *M. mercenaria* larval shell acquired using the 60× water immersion objective. The spectral peak at wavenumber 1131 is attributed to shell pigments previously reported for this species [19]. (*f*) Raman spectra of a *C. virginica* larval shell. (*g*) Raman spectra of a *C. gigas* larval shell.

(*M. edulis*-like). At the onset of calcification during the trochophore stage (21 hpf), we observed characteristic spectra for aragonite using *in vivo* CRM analyses (figure 1). To our knowledge, this is the first *in vivo* phase identification in a mollusc species, and during early shell deposition (trochophore stage). This developmental point was chosen for analyses since previous work has demonstrated that mussel larvae do not accumulate calcium carbonate prior to this developmental time point [14]. Our data do not provide evidence for the presence of amorphous precursors during larval calcification in Baltic *M. edulis*-like, although we analysed the larval shell at the earliest time point possible (trochophore stage). In addition, cross-sections of juvenile Baltic *M. edulis*-like shells reveal a distinctive separation between aragonitic and calcitic areas. Raman scans of juvenile shells with a sub-micron scale spatial resolution provide no evidence for ACC in the region close to the outer organic layer (periostracum) as observed previously for two freshwater adult bivalve species, *Hyriopsis cumingii* and *Diplodon chilensis* using Raman spectroscopy and FIB-TEM, high-resolution TEM and electron energy-loss spectroscopy methods [40]. The FTIR spectra collected from larval shells also exhibited only characteristic bands of aragonite with ν_4 and ν_2 bands at 713 cm^{-1} and 860 cm^{-1}, respectively (figure 6). As we could demonstrate that we are able to detect small quantities of ACC in ACC–aragonite mixtures (figure 2), we are confident that we would have detected ACC if it had been present. Other investigators have determined ACC in biological samples using CRM, including marine taxa, which further lends support to our methods [28,44–46].

Our findings suggest that the rapid calcification of PD I in Baltic *M. edulis*-like larvae may arise from the direct deposition of aragonite. The absence of ACC phases and direct deposition of crystalline phases has also been proposed for initial shell formation in bivalve larvae [25,26], nacre formation in adult molluscs [47] and the polychaete larval tubeworms, *Hydroides elegans* [48]. The rapid precipitation of a crystalline shell supports the necessity for a rigid external skeleton during larval development in bivalves. Rapid PD I shell formation enables muscle attachment and lateral compression of the larval body for swimming and feeding [49]. Our results indicate that the observed sensitivity of larval bivalves to ocean acidification stress [1,2,4,5] is not related to the presence of high amounts of ACC, which is more soluble than aragonite. Rather, the high sensitivity of larval bivalves to acidification may be associated with the reduced ability of these organisms to modulate the carbonate chemistry of their calcification space [14], limited maternally derived energy reserves [2] and the very high rates of shell deposition during that life stage [2,49].

Our results conflict with those of Weiss *et al*. [24], as we could not detect ACC in veliger shells. We attribute these differences to a number of factors. First, it has to be pointed out that in the study of Weiss *et al*. [24], the identification of ACC in *M. mercenaria* larval shells was based on the presence of the Raman peak at 1087 rel. cm^{-1}, which is an incorrect assignment. For calcite and aragonite, 1087 rel. cm^{-1} is the typical peak position , whereas the ACC peak is characteristically about 8 rel. cm^{-1} lower (1079 rel. cm^{-1}) [28,32]. Second, weak peaks or absence of peaks at 156 and 205 rel. cm^{-1} (lattice modes) and analyses of peak intensity ratios of the lattice mode (205 rel. cm^{-1}) and ν_1 peak (1086 rel. cm^{-1}) have been attributed to the presence of ACC phases in veliger larval mollusc shells [24]. However, weak peaks at 156 and 205 rel. cm^{-1} can be related to high background-to-signal ratio. Additionally, peak intensities at 156 and 205 rel. cm^{-1} are influenced by the orientation of crystallites [50]. This is illustrated by figure 4*a*,*b*,*d*, where we analysed the same

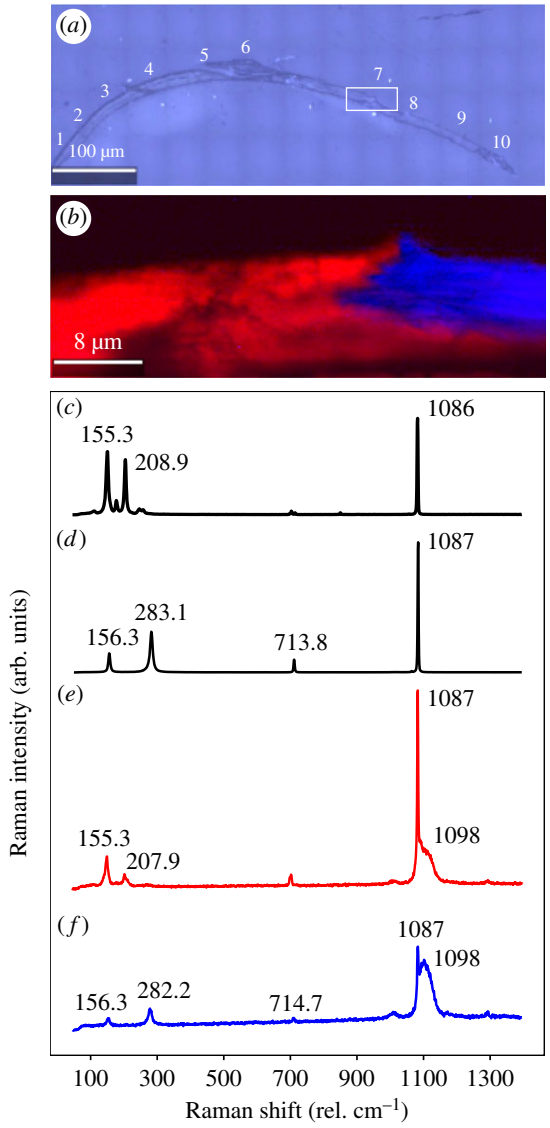

Figure 5. Juvenile shell deposition in Baltic *Mytilus edulis*-like using CRM. (*a*) Transmission image of a resin-embedded juvenile shell. The boxed region was subjected to a Raman scan. (*b*) Raman scan for the boxed region in (*a*) was integrated for CO_3^{2-}-stretching mode (1081.3–1091.3 rel. cm^{-1}, in red) and calcite lattice mode (268.4–298.4 rel. cm^{-1}, in blue). (*c*) Raman spectrum of an aragonite standard. (*d*) Raman spectrum of a calcite standard. (*e*) Raman spectrum of the juvenile shell in (*a*) at point 7. (*f*) Raman spectrum of the juvenile shell in (*a*) at point 8.

M. mercenaria larval shell with different objectives: the switch from a 20× to a 60× water immersion objective with a high numerical aperture reduces the background to signal ratios of Raman spectra. An important consideration during CRM analyses is the focal plane spectra are collected due to the presence of peaks at similar wavenumbers in water and ACC spectra (broad peak between wavenumbers 100–300 rel. cm^{-1}). However, the spectra for water are not accompanied by a v_1 peak for carbonate, as observed for ACC (figure 4*c*). We re-analysed both species studied by Weiss *et al.* ([24], *M. mercenaria*, *C. gigas*) and could not confirm the presence of ACC in their shells using our improved technical set-up. Instead, we were able to detect aragonite exclusively as the major carbonate phase in D-veliger shells. Additionally, we observe Raman spectra characteristic of aragonite at the outer surface of the larval shell (figure 4*d*) and also in the inner layer of approximately 3–5-µm thick shells. Based on previous structural observations using scanning electron microscopy, the granular structure of the inner bivalve larval shell was inferred to consist of ACC precursors [24]. We demonstrate that the previously reported structural differences in bivalve larval shell layers are not associated with a change in calcium carbonate polymorph composition. By using a 488 nm laser to reduce intrinsic fluorescence, we could acquire Raman spectra in both, *M. mercenaria* and *C. gigas* shells (figure 4*f–g*). For *C. gigas* shells, Weiss *et al.* [24] suggested that the peak height ratio of FTIR peaks at 856 cm^{-1}/713 cm^{-1} points towards the presence of ACC in larval shells. However, such ratios have been empirically demonstrated to be influenced by particle size [51] similar to particle sizes previously reported for ACC in larval shells [24] thus are not diagnostic for ACC. In addition, the presence of a peak at 713 cm^{-1} in FTIR spectra is a characteristic of crystalline calcium carbonate polymorphs [44] and the assignment of amorphous phases using FTIR in other marine taxa is based solely on the lack of a peak at 713 cm^{-1} [42,52]. Controlled ACC crystallization experiments by the addition of water clearly demonstrate the appearance of a v_4 peak at 712 cm^{-1} in FTIR spectra [53].

Recently, it has been suggested that molluscan larvae may use seed crystals to initiate shell formation based on empirical data from a FIB-TEM study on the D-veliger larvae of *P. fucata* [26]. FIB-TEM techniques have been demonstrated to suitably identify the presence of ACC in biological [54,55] and synthetic samples [56], avoiding laser-induced transformation of ACC or cryogenic sample preparation. This novel model for larval shell formation suggests the direct precipitation of seed crystals onto the organic matrix, which subsequently induces the inorganic precipitation of carbonate mineral. Based on these observations and our findings, we suggest that the direct deposition of aragonite may be an alternative mechanism for initial shell formation in bivalve larvae. Alternatively, the formation of ACC precursors that transform rapidly into a crystalline phase during larval calcification cannot be excluded, as we would have not been able to detect such a phenomenon with our methods. For example, DeVol *et al.* [57] observed ACC to be localized to small regions of the surface of nacre tablets in the abalone, *Haliotis rufescens* using nanometre resolution methods, photoemission electron spectromicroscopy (PEEM) and X-ray absorption near-edge structure (XANES) spectroscopy. In summary, evidence from the present study suggests that the major stable mineral phase during biomineralization in Baltic *M. edulis*-like larvae and juveniles, as well as other bivalve larvae, is crystalline calcium carbonate and not ACC.

4.2. Pigments in the shell

We show that prior to mineral deposition at 21 hpf, CRM analyses of larvae between 18 and 21 hpf reveal characteristic spectra for organic pigments in the region of the shell field (figure 1*d*). These peaks are located at 1158 and 1524 rel. cm^{-1}, which are characteristic peaks for carotenoid pigments attributed to the carbon–carbon double bond stretching mode and the carbon–carbon in-plane single bond stretching mode ,respectively (figure 1*d*, [58,59]). The presence of carotenoids in molluscs is widely reported for soft tissues, shells and pearls with putative roles of these molecules in mollusc defence and crystallography [34,60,61]. The spectral position of Raman peaks for organic pigments, such

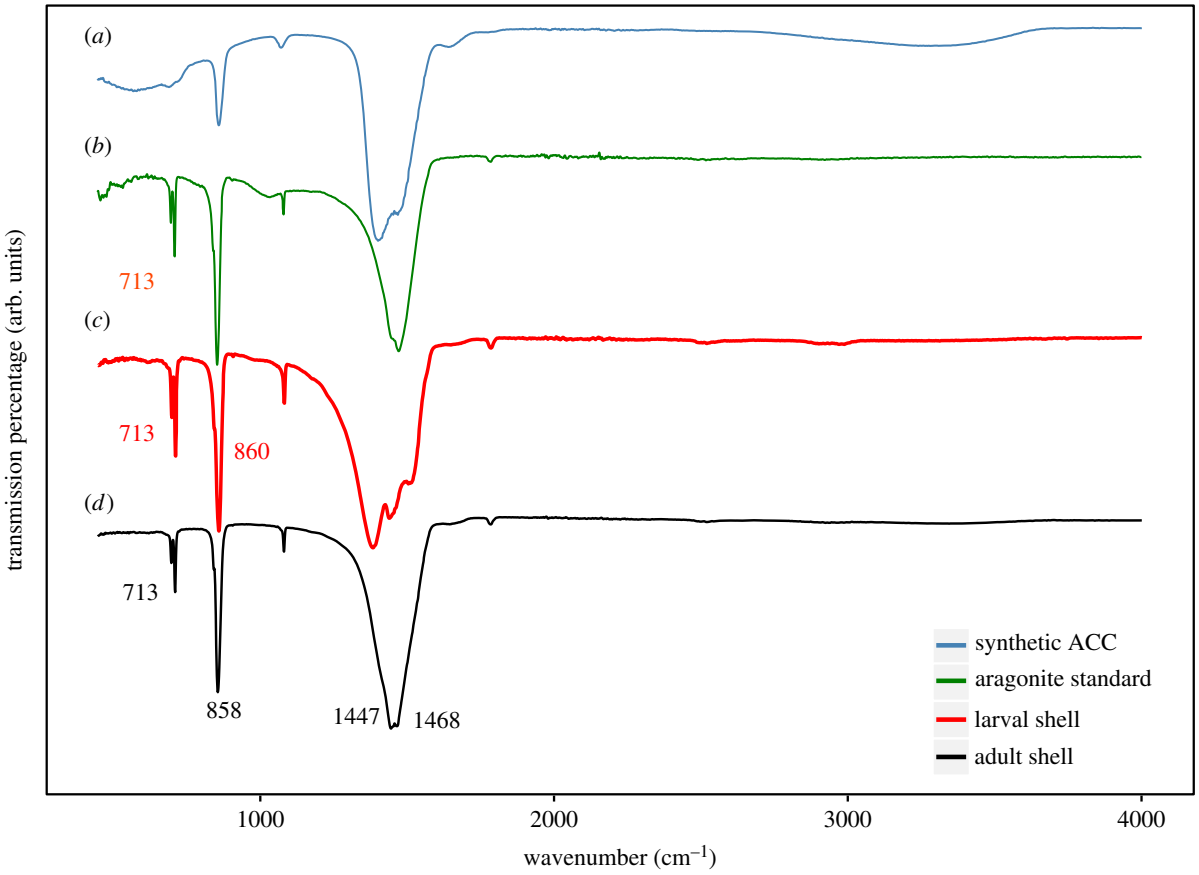

Figure 6. FTIR spectra of Baltic *M. edulis*-like larval shells. (*a*) FTIR spectrum of an ACC standard. (*b*) FTIR spectrum of an aragonite standard. (*c*) FTIR spectrum of D-veliger Baltic *M. edulis*-like shells. (*d*) FTIR spectrum of aragonite from an adult Baltic *M. edulis*-like shell.

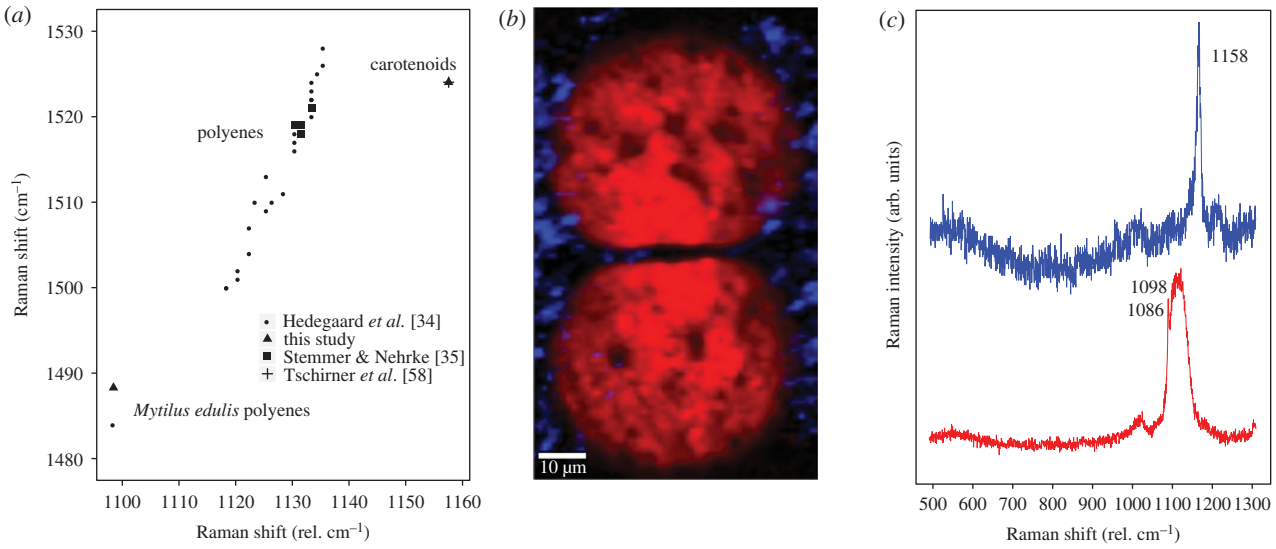

Figure 7. Presence of pigment polyenes in larval shells of Baltic *M. edulis*-like using CRM. (*a*) Plot of the relative wavenumbers for pigment polyenes measured in the shells several mollusc species. Data presented from Hedegaard *et al*. [34], Stemmer & Nehrke [35] and Tschirner *et al*. [58]. (*b*) Raman scan for the boxed region in figure 1*e* was integrated for CO_3^{2-}-stretching mode and Baltic *M. edulis*-like shell polyene (1076–1146 rel. cm^{-1}, in red) and carotenoids (1150.5–1170.5 rel. cm^{-1}, in blue). (*c*) Raman spectra for carotenoids around the growing edge of the shell (blue) and the larval shell and associated polyenes (red).

as carotenoids and polyenes, relates to the structure and composition of these molecules, defined by the carbon–carbon bonds [33]. A comparison of our data with previous data for carotenoid pigments and polyenes in *M. edulis* and other species is given in figure 7*a* [34,35,58]. Note the distinctly different grouping of polyenes (shifted to smaller wavenumbers) in comparison to carotenoid pigments, where the peaks recorded in the present study prior to calcification fall in line with characteristic organic peaks for β-carotene in figure 7*a*. In calcifying 21 hpf larvae, spectra for carotenoid pigments are recorded on the surface of the larval body, whereas characteristic organic peaks for *M. edulis* polyene pigments around 1098 rel. cm^{-1} as reported by Hedegaard *et al*. [34] are only observed when calcium

carbonate is incorporated (figure 7*c*), suggesting that these carotenoid pigments undergo structural changes when they are incorporated into the mineral phase. Despite the established association of polyene pigments in molluscan shells, there is no information on the mechanisms of shell pigment formation for any mollusc species. In corals, the structural transformation of polyenes within mineralized structures has been demonstrated by Maia *et al*. [62], where demineralization resulted in shifts of the polyene peaks, related to changes in the composition of double and single carbon bonds of pigments. Gene expression analyses for one shell protein (ependymin-related protein) revealed a strong correlation to shell pigmentation in the tropical abalone, *Haliotis asinina* [63]. These authors suggest that changes in the composition of polyenes during calcification may be linked to the formation of organic complexes with shell matrix proteins [63]. The formation of such organic complexes between calcium carbonate and carotenoids has been reported for the hydrocoral *Errina antarctica* [64]. To our knowledge, this is the first report of Raman spectral shift of organic pigments in the shell of the Baltic *M. edulis*-like larvae. Such Raman shifts may be attributed to structural transformation (C=C and C–C bonds) from carotenoid pigments to the species-specific pigment polyenes previously reported for *M. edulis* [34]. The conversion of carotenoids to species-specific shell polyenes may be a conserved mechanism and further analysis of pigments during the course of calcification in other mollusc species is needed to investigate this possibility.

5. Conclusion

(1) Initial crystal formation occurs during the swimming, trochophore stage observed using techniques suitable for the detection of ACC in biological samples.
(2) From the onset of calcification to the formation of the juvenile shell, there is no evidence for ACC precursors in Baltic *M. edulis*-like larvae using *in vivo* confocal Raman and FTIR spectroscopy.
(3) During larval shell formation, polyenes are deposited within the shell that may derive form the structural transformation of carotenoid pigments, which are present within the shell field area prior to the formation of the mineral phase.

Data accessibility. All data are available via the PANGAEA repository (https://doi.org/10.1594/PANGAEA.887420).

Authors' contributions. K.R. and F.M. designed the study and maintained larval cultures. A.G. and C.G. cultured and provided samples of *Mercenaria mercenaria* and *Crassostrea virginica*. K.R., G.N. and F.M. collected data and wrote the manuscript. K.R. and G.N. analysed the data. C.R. and D.T. supported FTIR measurements. All authors commented on the manuscript and gave their final approval for publication.

Competing interests. We declare we have no competing interests.

Funding. This study is funded by the European Union's Seventh Framework Programme [FP7] ITN project 'CACHE' under REA grant agreement no. [605051]13.

Acknowledgements. The authors thank Ms Cornelia Ulrich for her technical support during FTIR measurements.

References

1. Thomsen J, Haynert K, Wegner KM, Melzner F. 2015 Impact of seawater carbonate chemistry on the calcification of marine bivalves. *Biogeosciences* **12**, 4209–4220. (doi:10.5194/bg-12-4209-2015)
2. Waldbusser G, Brunner EL, Haley B., Hales B, Langdon CJ, Prahl FG. 2013 A developmental and energetic basis linking larval oyster shell formation to acidification sensitivity. *Geophys. Res. Lett.* **40**, 2171–2176. (doi:10.1002/grl.50449)
3. Frieder CA, Applebaum SL, Pan TCP, Hedgecock D, Manahan DT. 2017 Metabolic cost of calcification in bivalve larvae under experimental ocean acidification. *ICES J. Mar. Sci.* **74**, 941–954.
4. Kurihara H. 2008 Effects of CO_2-driven ocean acidification on the early developmental stages of invertebrates. *Mar. Ecol. Prog. Ser.* **373**, 275–284. (doi:10.3354/meps07802)
5. Gazeau F, Parker LM, Comeau S, Gattuso JP, O'Connor WA, Martin S, Portner HO, Ross PM. 2013 Impacts of ocean acidification on marine shelled molluscs. *Mar. Biol.* **160**, 2207–2245. (doi:10.1007/s00227-013-2219-3)
6. Mette MJ, Wanamaker AD, Carroll ML, Ambrose WG, Retelle MJ. 2016 Linking large-scale climate variability with *Arctica islandica* shell growth and geochemistry in northern Norway. *Limnol. Oceanogr.* **61**, 748–764. (doi:10.1002/lno.10252)
7. Waldbusser GG, Hales B, Langdon CJ, Haley BA, Schrader P, Brunner EL, Gray MW, Miller CA, Giminez I. 2015 Saturation-state sensitivity of marine bivalve larvae to ocean acidification. *Nat. Clim. Change.* **5**, 273–280. (doi:10.1038/nclimate2479)
8. Waldbusser GG *et al.* 2015 Ocean acidification has multiple modes of action on bivalve larvae. *PLoS ONE* **10**, e0128376. (doi:10.1371/journal.pone.0128376)
9. Marali S, Schone BR, Mertz-Kraus R, Griffin SM, Wanamaker AD, Matras U, Butler PG. 2017 Ba/Ca ratios in shells of *Arctica islandica*—potential environmental proxy and crossdating tool. *Palaeogeogr. Palaeoclimatol. Palaeoecol.* **465**, 347–361. (doi:10.1016/j.palaeo.2015.12.018)
10. Kniprath E. 1981 Ontogeny of the molluscan shell field: a review. *Zool. Scri.* **10**, 61–79. (doi:10.1111/j.1463-6409.1981.tb00485.x)
11. Kniprath E. 1978 Growth of shell-field in *Mytilus* (Bivalvia) *Zool. Scripta.* **7**, 119–120. (doi:10.1111/j.1463-6409.1978.tb00594.x)
12. Kin K, Kakoi S, Wada H. 2009 The novel role of *dpp* in the shaping of bivalve shells revealed in a conserved molluscan developmental program. *Dev. Biol.* **329**, 152–166. (doi:10.1016/j.ydbio.2009.01.021)
13. Eyster LS. 1983 Ultrastructure of early embryonic shell formation in the opisthobranch gastropod *Aeolidia papillosa*. *Biol. Bull.* **165**, 394–408. (doi:10.2307/1541204)
14. Ramesh K, Hu MY, Thomsen J, Bleich M, Melzner F. 2017 Mussel larvae modify calcifying fluid carbonate chemistry to promote calcification. *Nat. Comm.* **8**, 1709. (doi:10.1038/s41467-017-01806-8)
15. Aranda-Burgos JA, Da Costa F, Novoa S, Ojea J, Martinez-Patino D. 2014 Embryonic and larval development of *Ruditapes decussatus* (Bivalvia: Veneridae): a study of the shell differentiation process. *J. Molluscan Stud.* **80**, 8–16. (doi:10.1093/mollus/eyt044)
16. Iwata K. 1980 Mineralization and architecture of the larval shell of *Haliotis discus* hannai Ino, (Archaeogastropoda). *J. Fac. Sci.* **19**, 305–320.
17. Castilho F, Machado J, Reis ML, Sá C. 1989 Ultrastructural study of the embryonic and larval shell of *Anodonta cygnea*. *Can. J. Zool.* **67**, 1659–1664. (doi:10.1139/z89-238)
18. Medakovic D, Popovic S, Grzeta B, Plazonic M, Hrs-Brenko M. 1997 X-ray diffraction study of calcification processes in embryos and larvae of the brooding oyster *Ostrea edulis*. *Mar. Biol.* **129**, 615–623. (doi:10.1007/s002270050204)
19. Thompson CM, North EW, White SN, Gallager SM. 2014 An analysis of bivalve larval shell pigments using micro-Raman spectroscopy. *J. Raman Spectrosc.* **45**, 349–358. (doi:10.1002/jrs.4470)
20. Kniprath E. 1980 Larval development of the shell and the shell gland in *Mytilus* (Bivalvia). *Roux. Arch. Dev. Biol.* **188**, 201–204. (doi:10.1007/BF00849049)
21. Griesshaber E, Wolfgang W, Ubhi HS, Huber J, Nindiyasari F, Maier BJ, Ziegler A. 2013

Homoepitaxial meso- and microscale crystal co-orientation and organic matrix network structure in *Mytilus edulis* nacre and calcite. *Acta Biomater.* **9**, 9492–9502. (doi:10.1016/j.actbio.2013.07.020)

22. Weiner S, Addadi L. 2011 Crystallization pathways in biomineralisation. *Annu. Rev. Mater. Res.* **41**, 21–40. (doi:10.1146/annurev-matsci-062910-095803)
23. Vidavsky N, Addadi S, Mahamid J, Shimoni E, Ben-Ezra D, Shpigel M, Weiner S, Addadi L. 2014 Initial stages of calcium uptake and mineral deposition in sea urchin embryos. *Proc. Natl Acad. Sci. USA* **111**, 39–44. (doi:10.1073/pnas.1312833110)
24. Weiss I, Tuross N, Addadi L, Weiner S. 2002 Mollusc larval shell formation: amorphous calcium carbonate is a precursor phase for aragonite. *J. Exp. Zool.* **293**, 478–491. (doi:10.1002/jez.90004)
25. Kudo M, Kameda J, Saruwatari K, Ozaki N, Okano K, Nagasawa H, Kogure T. 2010 Microtexture of larval shell of oyster, *Crassostrea nippona*: a FIB-TEM study. *J. Struct. Biol.* **169**, 1–5. (doi:10.1016/j.jsb.2009.07.014)
26. Yokoo N, Suzuki M, Saruwatari K, Aoki H, Watanabe K, Nagasawa H, Kogure T. 2011 Microstructures of the larval shell of a pearl oyster, *Pinctada fucata*, investigated by FIB-TEM technique. *Am. Mineral.* **96**, 1020–1027. (doi:10.2138/am.2011.3657)
27. Addadi L, Raz S, Weiner S. 2003 Taking advantage of disorder: amorphous calcium carbonate and its roles in biomineralisation. *Adv. Mater.* **15**, 959–970. (doi:10.1002/adma.200300381)
28. Raz S, Testeniere O, Hecker A, Weiner S, Luquet G. 2002 Stable amorphous calcium carbonate is the main component of the calcium storage structures of the crustacean *Orchestia cavimana*. *Biol. Bull.* **203**, 269–274. (doi:10.2307/1543569)
29. Stuckas H, Knöbel L, Schade H, Breusing C, Hinrichsen HH, Bartel M, Langguth K, Melzner F. 2017 Combining hydrodynamic modelling with genetics: can passive larval drift shape the genetic structure of Baltic *Mytilus* populations? *Mol. Ecol.* **26**, 2765–2782. (doi:10.1111/mec.14075)
30. Barton A, Hales B, Waldbusser GE, Langdon C, Feely RA. 2012 The Pacific oyster, *Crassostrea gigas*, shows negative correlation to naturally elevated carbon dioxide levels: implications for near-term ocean acidification effects. *Limnol. Oceanogr.* **57**, 698–710. (doi:10.4319/lo.2012.57.3.0698)
31. Talmage S, Gobler C. 2009 The effects of elevated carbon dioxide concentrations on the metamorphosis, size and survival or larval hard clams (*Mercenaria mercenaria*), bay scallops (*Argopecten irradians*), and Eastern oysters (*Crassostrea virginica*). *Limnol. Oceanogr.* **54**, 2072–2080. (doi:10.4319/lo.2009.54.6.2072)
32. Rodriguez-Blanco JD, Shaw S, Benning LG. 2008 How to make 'stable' ACC: protocol and preliminary structural characterization. *Mineral. Mag.* **72**, 283–286. (doi:10.1180/minmag.2008.072.1.283)
33. Kranz SA, Wolf-Gladrow D, Nehrke G, Langer G, Rost B. 2010 Calcium carbonate precipitation induced by the growth of the marine cyanobacterium *Trichodesmium*. *Limnol. Oceanogr.* **55**, 2563–2569. (doi:10.4319/lo.2010.55.6.2563)
34. Hedegaard C, Bardeau JF, Chateigner D. 2006 Molluscan shell pigments: an *in situ* resonance Raman study. *J. Molluscan Stud.* **72**, 157–162. (doi:10.1093/mollus/eyi062)
35. Stemmer K, Nehrke G. 2014 The distribution of polyenes in the shell of *Arctica islandica* from North Atlantic localities: a confocal Raman microscopy study. *J. Molluscan Stud.* **80**, 365–370. (doi:10.1093/mollus/eyu033)
36. Nehrke G, Poigner H, Wilhems-Dick D, Brey T, Abele D. 2012 Coexistence of three calcium carbonate polymorphs in the shell of the Antarctic clam *Laternula elliptica*. *Geochem. Geophys. Geosyst.* **13**, 1–8. (doi:10.1029/2011GC003996)
37. Wall M, Nehrke G. 2012 Reconstructing skeletal fiber arrangement and growth mode in the coral *Porites lutea* (Cnidaria, Scleractinia): a confocal Raman microscopy study. *Biogeosciences* **9**, 4885–4895. (doi:10.5194/bg-9-4885-2012)
38. Schonitzer V, Weiss IM. 2007 The structure of mollusc larval shells formed in the presence of the chitin synthase inhibitor Nikkomycin Z. *BMC Struct. Biol.* **7**, 71. (doi:10.1186/1472-6807-7-71)
39. Urmos J, Sharma SK, Mackenzie FT. 1991 Characterization of some biogenic carbonates with Raman spectroscopy. *Am. Mineral.* **76**, 641–646.
40. Jacob DE, Wirth R, Soldati AL, Wehrmeister U, Schreiber A. 2011 Amorphous calcium carbonate in the shells of adult Unionoida. *J. Struct. Biol.* **173**, 241–249. (doi:10.1016/j.jsb.2010.09.011)
41. Anderson FA, Brecevic L. 1991 Infrared spectra of amorphous and crystalline calcium carbonate. *Acta Chem. Scand.* **45**, 1018–1024. (doi:10.3891/acta.chem.scand.45-1018)
42. Aizenberg J, Lambert G, Weiner S, Addadi L. 2002 Factors involved in the formation of amorphous and crystalline calcium carbonate: a study of an ascidian skeleton. *J. Am. Chem. Soc.* **124**, 32–39. (doi:10.1021/ja016990l)
43. Hodson ME, Benning LG, Demarchi B, Penkman KEH, Rodriguez-Blanco JD, Schofield PF, Versteegh EAA. 2015 Biomineralisation by earthworms—an investigation into the stability and distribution of amorphous calcium carbonate. *Geochem. Trans.* **16**, 4. (doi:10.1186/s12932-015-0019-z)
44. Hild S, Marti O, Ziegler A. 2008 Spatial distribution of calcite and amorphous calcium carbonate in the cuticle of the terrestrial crustaceans *Porcellio scaber* and *Armadillidium vulgare*. *J. Struct. Biol.* **163**, 100–108. (doi:10.1016/j.jsb.2008.04.010)
45. Weiner S, Levi-Kalisman Y, Raz S, Addadi L. 2003 Biologically formed amorphous calcium carbonate. *Connect. Tissue Res.* **44**, 214–218. (doi:10.1080/03008200390181681)
46. Wehrmeister U, Jacob DE, Soldati AL, Loges N, Häger T, Hofmeister W. 2010 Amorphous, nanocrystalline and crystalline calcium carbonates in biological materials. *J. Raman Spectrosc.* **42**, 926–935. (doi:10.1002/jrs.2835)
47. Saruwatari K, Matsui T, Mukai H, Nagasawa H, Kogure T. 2009 Nucleation and growth of aragonite crystals at the growth front of nacres in pearl oyster, *Pinctada fucata*. *Biomaterials* **30**, 3028–3034. (doi:10.1016/j.biomaterials.2009.03.011)
48. Chan VBS, Toyofuku T, Wetzel G, Saraf L, Thiyagarajan V, Mount AS. 2015 Direct deposition of crystalline aragonite in the controlled biomineralization of the calcareous tubeworm. *Front. Mar. Sci.* **2**, 97. (doi:10.3389/fmars.2015.00097)
49. Galtsoff PS. 1964 *The American oyster,* Crassostrea virginica *Gmelin. Chapter 16: Larval development and metamorphosis*. *Fishery Bulletin*, pp. 355–380. North East Fishery Science Centre.
50. Nehrke G, Nouet J. 2011 Confocal Raman microscope mapping as a tool to describe different mineral and organic phases at high spatial resolution within marine biogenic carbonates: case study on *Nerita undata* (Gastropoda, Neritopsina). *Biogeosciences* **8**, 3761–3769. (doi:10.5194/bg-8-3761-2011)
51. Kristova P, Hopkinson LJ, Rutt KJ. 2015 The effect of the particle size on the fundamental vibrations of the $[CO_3^{2-}]$ anion in calcite. *J. Phys. Chem. A* **119**, 4891–4897. (doi:10.1021/acs.jpca.5b02942)
52. Salter MA, Harborne AR, Perry CT, Wilson RW. 2017 Phase heterogeneity in carbonate production by marine fish influences their roles in sediment generation and the inorganic carbon cycle. *Sci. Rep.* **7**, 765. (doi:10.1038/s41598-017-00787-4.
53. Khouzani MF, Chevrier DM, Guettlein P, Hauser K, Zhang P, Hedin N, Gebauer D. 2015 Disordered amorphous calcium carbonate from direct precipitation. *Cryst. Eng. Comm.* **17**, 4842–4849. (doi:10.1039/C5CE00720H)
54. Hikida T, Nagasawa H, Kogure T. 2003 Characterization of amorphous calcium carbonate in the gastrolith of cray fish, *Procambarus clarkia*. In *Biomineralization* (*BIOM2001*) (eds I Kobayashi, H Ozawa), pp. 81–84. Kanagawa, Japan: Tokai University Press.
55. Yokoo N. 2012 *Investigation of amorphous calcium carbonate* (*ACC*) *in biomineralisation*. Department of Earth and Planetary Science. The University of Tokyo Graduate School of Science.
56. Suzuki M, Nagasawa H, Kogure T. 2006 Synthesis and structure of hollow calcite particles. *Cryst. Growth Des.* **6**, 2004–2006. (doi:10.1021/cg0602921)
57. DeVol RT, Sun CY, Marcus MA, Coppersmith SN, Myneni SCB, Gilbert PUPA. 2015 Nanoscale transforming mineral phases in fresh nacre. *J. Am. Chem. Soc.* **137**, 13 325–13 333. (doi:10.1021/jacs.5b07931)
58. Tschirner N, Schenderlein M, Brose K, Schlodder E, Mroginski MA, Hildebrandt P, Thomse, C. 2008 Raman excitation profiles of β-carotene—novel insights into the nature of the ν_1-band. *Phys. Status Solidi B.* **245**, 2225–2228. (doi:10.1002/pssb.200879649)
59. Baranska M, Romana M, Dobrowolski J, Schulz H, Baranski R. 2013 Recent advances in Raman analysis of plants: alkaloids, carotenoids, and polyacetylenes.

Curr. Anal. Chem. **9**, 108–127. (doi:10.2174/157341113804486455)

60. Matsuno T, Hirao S. 1989 Marine carotenoids. In *Marine biogenic lipids, fats, and oils*, vol. 1 (ed. RG Ackman), pp. 251–388. Boca Raton, FL: CRC Press.
61. Vershinin A. 1996 Carotenoids in mollusca: approaching the functions. *Comp. Biochem. Physiol. B. Biochem. Mol. Biol.* **133**, 63–71. (doi:10.1016/0305-0491(96)00104-6)
62. Maia LF, de Oliveira VE, Oliveira MER, Reis FD, Fleury BG, Edwards HGM, de Oliveira LFC. 2013 Colour diversification in octocorals based on conjugated polyenes: a Raman spectroscopic view. *J. Raman Spectrosc.* **44**, 560–566. (doi:10.1002/jrs.4226)
63. Jackson DJ, Wörheide G, Degnan BM. 2007 Dynamic expression of ancient and novel molluscan shell genes during ecological transitions. *BMC Evol. Biol.* **7**, 160. (doi:10.1186/1471-2148-7-160)
64. Czeczuga B. 1985 Carotenoid–calcium carbonate complex from the hydrocoral *Errina antarctica*. *Biochem. Syst. Ecol.* **13**, 455–457. (doi:10.1016/0305-1978(85)90092-4)